# TWO-DIMENSIONAL EXCITON SUPERPOSITION STATES WITH DIRAC CONE DISPERSION LAWS

**S. A. Moskalenko, I. V. Podlesny, and I. A. Zubac**

*Institute of Applied Physics, Academiei str. 5, Chisinau, MD-2028, Republic of Moldova*
*E-mail: exciton@phys.asm.md*

(Received July 17, 2019)

## Abstract

Our review paper is dedicated to studies of two-dimensional (2D) Wannier–Mott excitons in transition metal dichalcogenides and 2D magnetoexcitons in GaAs-type quantum wells subjected to the action of a strong perpendicular magnetic field, which both revealed the Dirac cone dispersion laws. It is shown that necessary conditions for the implementation of this property to be carried out are the taking into account of the electron–hole (e–h) exchange Coulomb interaction and the interdependence between the center-of-mass and relative e–h motions in the frame of the excitons. A short review describing the effect of these two factors on the Dirac cone dispersion law formation is presented.

## 1. Introduction

To date, two types of the 2D excitons with Dirac cone dispersion laws have been elucidated. One of them concerns the Wannier–Mott excitons in transition metal dichalcogenides (TMDCs), such as molybdenum and wolfram monolayers $MoX_2$ and $WX_2$ with X=S, Se [1]. The other type of excitons can be formed in GaAs quantum wells (QWs) subjected to the action of a strong perpendicular magnetic field [2]. Below, a short review of these two variants is presented. In both cases, the arising of the Dirac cone dispersion laws takes place under the influence of the electron–hole (e–h) exchange Coulomb interaction under conditions, where the interdependence between the center-of-mass and the relative e–h motions does appear. The linear dispersion law of the 2D Bose gas is a rare case. It can change the thermodynamic properties of the system opening a possibility of achieving its Bose–Einstein condensation (BEC) at finite temperatures even at its infinite extent [3].

According to Hohenberg [4], in a homogeneous 2D Bose gas with parabolic dispersion laws, the quantum fluctuations arising on the surface with an infinite extent are able to destroy the establishing of the coherent macroscopic states. The BEC of 2D excitons at nonzero temperatures becomes impossible. To avoid this restriction, it was necessary to confine the surface of the gas. For example, in the case of 2D cavity exciton polaritons with parabolic dispersion law, their BEC at low yet finite temperatures was achieved via confining the excitons on the surface of the light spot created by a laser beam on the QW embedded into the microcavity [5, 6].

## 2. Band Structures of Two Exciton Systems

The band structure of dichalcogenide monolayers was described in [1]. This type of monolayers happens to be direct band gap semiconductors with minimal direct band gaps at the

corner points $\vec{K}$ and $-\vec{K}$ of the hexagonal Brillouin zone, as shown in Fig. 1. There are two valleys $\vec{K}$ and $-\vec{K}$, where the valence electrons effectuate direct optical quantum transitions in the conduction bands, while maintaining their spin projections. Due to the symmetry of the Hamiltonian as regards the time inversion in the structures without a center of inversion, the Kramers theorem establishes that the energy of electron with spin up in valley $\vec{K}$ equals to the energy of the electron with spin down in valley $-\vec{K}$. This property is shown in Fig. 1. Direct optical quantum transitions take place with the participation of photons with different circular polarizations. The bare Wannier–Mott excitons appearing in $\vec{K}$ and $-\vec{K}$ valleys due to the direct Coulomb e–h interactions have the same energies of their binding and creation. Two degenerate valley exciton states can be characterized by valley pseudospin projections.

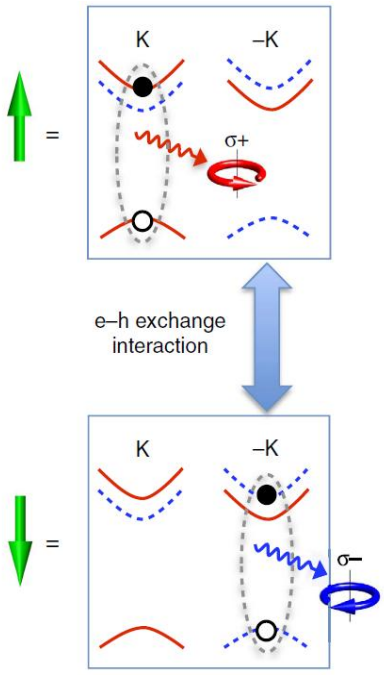


**Fig. 1.** Valley-orbit coupled exciton $X_0$. Valley pseudospin up and down configurations of $X_0$. The figure is reproduced from the paper of Yu. H. et al., Nat. Commun. 5, 3876 (2014).

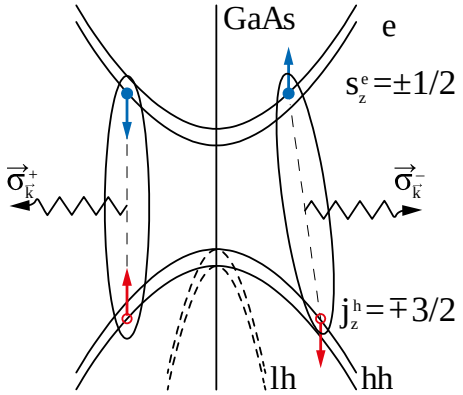


**Fig. 2.** Band structure of the GaAs crystal.

The band structure of GaAs QWs in the absence of an external perpendicular magnetic field is shown in Fig. 2. The conduction electrons have spin projections $s_z^e = \pm 1/2$, and the heavy holes have the full angular momentum projections $j_z^h = \pm 3/2$. Its origin is associated with the locking of the valence electron spin projection up (down) with the *p*-type orbit magnetic moment projection $M = 1(-1)$ giving rise to the resultant projections $3/2\,(-3/2)$, as shown in Fig. 3. The total angular momentum projection of the e–h pair $F = s_z^e + j_z^h$ is a quantum number characterizing the states of the e–h pairs and of the excitons. It has four possible values $F = \pm 1, \pm 2$. Two exciton states with $F = \pm 1$ are shown in Fig. 2. They can emit photons with different circular polarizations. As in the case of the TMDCs, in the case of GaAs QWs, there are two bare exciton degenerate states interacting with photons of different circular polarizations. A strong perpendicular magnetic field leads to the Landau quantization of the orbital motions and the formation of discrete energy levels of electrons and holes separately, as is shown in Fig. 4. Under the action of the Lorentz force, the magnetoexciton with in-plane wave vector $\vec{k}_{||}$ looks as an electric dipole, as is shown in Fig. 5.

$$\psi_{c,s,\pm 1/2,\vec{q}} = \frac{e^{i\vec{q}\vec{r}}}{\sqrt{V}} U_{c,s,\vec{q}}(\vec{r}) \begin{vmatrix} \uparrow \rangle \\ \downarrow \rangle \end{vmatrix}; \qquad \varphi_{n,p}(x,y) = \frac{e^{ipx}}{\sqrt{L_x}} \varphi_n\left(y - pl_0^2\right); \quad l_0^2 = \frac{\hbar c}{eB}$$

$$\psi_{v,p,3/2,3/2,\vec{q}} = \frac{e^{i\vec{q}\vec{r}}}{\sqrt{2V}} [U_{v,p,x,\vec{q}}(\vec{r}) + iU_{v,p,y,\vec{q}}(\vec{r})] \left| \uparrow \right\rangle;$$

$$\psi_{v,p,3/2,-3/2,\vec{q}} = \frac{e^{i\vec{q}\vec{r}}}{\sqrt{2V}} [U_{v,p,x,\vec{q}}(\vec{r}) - iU_{v,p,y,\vec{q}}(\vec{r})] \left| \downarrow \right\rangle;$$

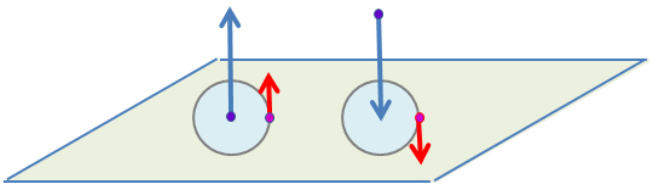

$$\vec{\sigma}_M = \frac{1}{\sqrt{2}}\left(\vec{a}_1 \pm i\vec{a}_2\right).$$

$$M = \pm 1$$

**Fig. 3.** Conduction and valence electron wave functions.

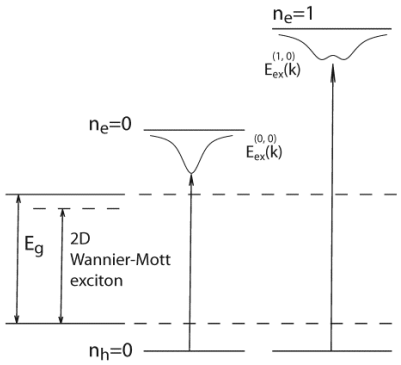


**Fig. 4.** Scheme of two magnetoexciton energy bands (reproduced from [7]).

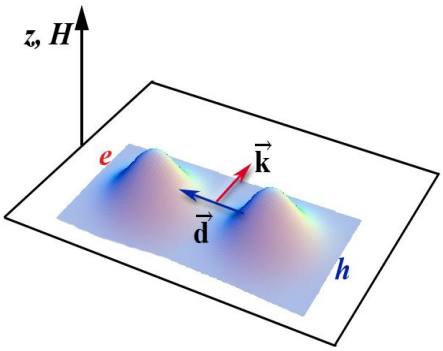


**Fig. 5.** Electric-dipole model of a 2D magnetoexciton with wave vector $\vec{k}$ and with the arm of the electric dipole moment $\vec{d}$ [8].

The binding energy and the ionization potential are determined by the direct Coulomb e–h interaction. The arm of the dipole is proportional to the center-of-mass wave vector yet perpendicular to it. Despite the change of the orbital structure of the magnetoexciton compared with the Wannier–Mott exciton with hydrogen atom-type structure, the spin structure of the magnetoexciton remains the same as in the absence of a magnetic field until the Rashba spin–orbit coupling (RSOC) is not taken into account. A new property of the 2D magnetoexciton is the interdependence between the center-of-mass and the relative e–h motions induced by the action of the Lorentz force. This interdependence happens to play an important role promoting to the formation of the Dirac cone dispersion law under the influence of the exchange e–h Coulomb interaction.

## 3. Electron–Hole Exchange Coulomb Interaction

The diagrams representing the direct, exchange, and mixed e–h Coulomb interactions are shown in Fig. 6. During the direct Coulomb scattering, the particles are moving separately without changing their origins. In the exchange scattering process, the e–h pairs are created and annihilated. In the case of the valley excitons in the TMDCs, these processes can take place with the electron from one valley and with the hole from another valley, which can lead to the interdependence between the center-of-mass and the relative e–h motions even in the absence of an external perpendicular magnetic field. In both cases, the exchange e–h Coulomb interaction removes the degeneracy of the bare exciton states and leads to the formation of their coherent superposition states with well-defined coefficients of linear combinations. These superposition states in the case of two valley exciton states were shown in [1]. One of them has a Dirac cone dispersion law, whereas the other state has a Kirgiz hat-type dispersion law with minimum energy on the circle formed by the in-plane wave vectors, as shown in Fig. 7.

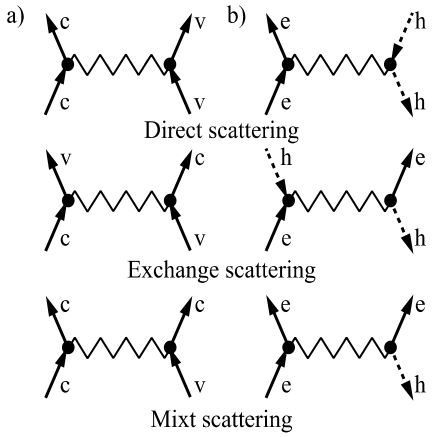


**Fig. 6.** Electron–hole Coulomb scattering processes: (a) in two-band representation and (b) in electron-hole description.

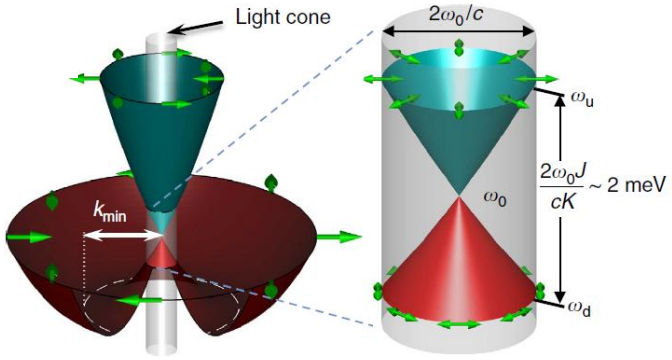


**Fig. 7.** Dispersion of valley-orbit coupled $X_0$, which in the light cone implements a massless Dirac cone with chirality index $l$=2. Figure is reproduced from the paper of Yu. H. et al., Nat. Commun. 5, 3876 (2014).

In the case of the 2D magnetoexcitons, the superposition states are described by formulas (1):

$$\left|\psi_0^{\pm}\right\rangle = c_1^{\pm}\left[\left|\psi_{ex}\left(-1;\vec{k}_{\|}\right)\right\rangle \pm e^{-2i\varphi}\left|\psi_{ex}\left(1;\vec{k}_{\|}\right)\right\rangle\right],$$

$$E_{ex}^{+}(\vec{k}_{\|}) = E_{ex}^{0}(\vec{k}_{\|}) + \varepsilon_0 + I_l\sqrt{\frac{2}{\pi}}\left|\frac{\rho_{c-v}}{l_0}\right|^2 e^{-\frac{|\vec{k}_{\|}|^2 l_0^2}{2}}\left|\vec{k}_{\|}\right| l_0.$$

$$E_{ex}^{-}(\vec{k}_{\|}) = E_{ex}^{0}(\vec{k}_{\|}) + \varepsilon_0; \quad \varepsilon_0 = -\frac{1}{2}I_l\left|\frac{\rho_{c-v}}{l_0}\right|^2; \quad l_0^2 = \frac{\hbar c}{eB}.$$

$$E_{ex}^{0}\left(\vec{k}_{\|}\right) = -I_l e^{-\frac{|\vec{k}_{\|}|^2 l_0^2}{4}} I_0\left(\frac{\left|\vec{k}_{\|}\right|^2 l_0^2}{4}\right); \quad I_l = \frac{e^2}{\varepsilon_0 l_0}\sqrt{\frac{\pi}{2}}, \tag{1}$$

$$\left|\Psi_1\right\rangle = \left|\Psi_{ex}(-1;\vec{k}_{\|})\right\rangle; \qquad \left|\Psi_2\right\rangle = \left|\Psi_{ex}(1;\vec{k}_{\|})\right\rangle.$$

The bare magnetoexciton states are determined by the quantum numbers $F = \pm 1$ in the way $|\Psi_1\rangle = |\Psi_{ex}(-1;\vec{k}_{\|})\rangle$; $|\Psi_2\rangle = |\Psi_{ex}(1;\vec{k}_{\|})\rangle$ and the superposition states are denoted as $|\Psi_0^{\pm}\rangle$. It is evident from Fig. 8 that the symmetric superposition state $|\Psi_0^{+}\rangle$ acquires a linear dispersion law in the range of in-plane wave vectors $\vec{k}_{\|} l_0 < 1$, where $l_0$ is the magnetic length. The asymmetric superposition state $|\Psi_0^{-}\rangle$ remains with the same dispersion law as the bare magnetoexciton states.

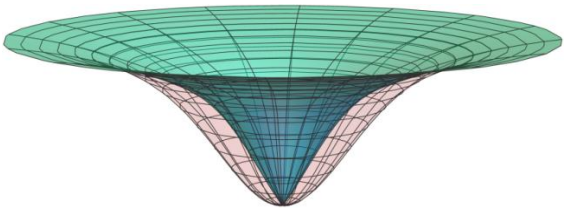

**Fig. 8.** Branches of 2D bright magnetoexciton in two superposition states with and without Dirac cone dispersion law.

The selection rules of the quantum transitions from the ground state of the crystal to the superposition states are discussed in the following section.

## 4. Selection Rules of the Optical Quantum Transitions

It is evident from Fig. 9 that the photons are propagating in any arbitrary direction of the 3D space, being characterized by circular polarizations $\vec{\sigma}_{\vec{k}}^{\pm}$. The 2D magnetoexcitons are located on the 2D plane of the layer. They are characterized by the quantum numbers $F = \pm 1$, what is equivalent to the circular polarization $\vec{\sigma}_M = (1/\sqrt{2})(\vec{a}_1 \pm i\vec{a}_2)$ with $F = M = \pm 1$. Here, $\vec{a}_1$ and $\vec{a}_2$ are the in-plane unit vectors. The selection rules of the quantum transitions from the ground state of the crystal to the superposition states depend essentially on quantum numbers $n_e$ and $n_h$ of the electron and hole Landau quantization levels. In the lowest Landau levels (LLLs) approximation, where only the lowest numbers $n_e = n_h = 0$ are taken into account, the geometric selection rules depend on the scalar products $(\vec{\sigma}_{\vec{k}}^{\pm} \cdot \vec{\sigma}_M^{*})$ in their different combinations. It was shown [2] that both superposition states are dipole active in the both circular polarizations. However, in the case of a symmetric state, the probability of the quantum transition depends on the direction of light propagation as regards the semiconductor layer. It has the dependence proportional to $k_z^2/|\vec{k}|^2$, where $\vec{k} = a_3 k_z + \vec{k}_{\|}$, and $a_3$ is the unit vector oriented perpendicular to the layer surface. It is maximal in the Faraday geometry with light wave vector $\vec{k}$ perpendicular to the surface of the layer and vanishes in the Voigt geometry with the light propagation along the layer surface. This dependence on light wave vector projection $k_z$ does not mean the appearance of a quadrupole quantum transition. It would be characterized by the quadratic dependence on the magnetoexciton in-plane wave vector $\vec{k}_{\|}$ and would be looking as $|\vec{k}_{\|}|^2 l_0^2$. In the case of an asymmetric superposition state, the probability of the quantum transition does not

depend on the direction of light propagation at all. These results are shown in Fig. 10.

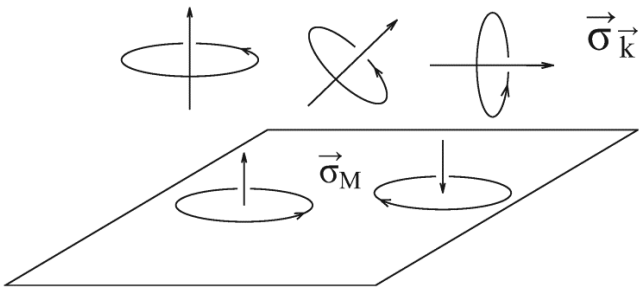


**Fig. 9.** Circular polarizations of the photons and the 2D excitons. The geometric selection rules are determined by factors $\left|(\vec{\sigma}^{\pm}_{\vec{k}} \cdot \vec{\sigma}^{*}_{M})\right|^2$. The figure is reproduced from [7].

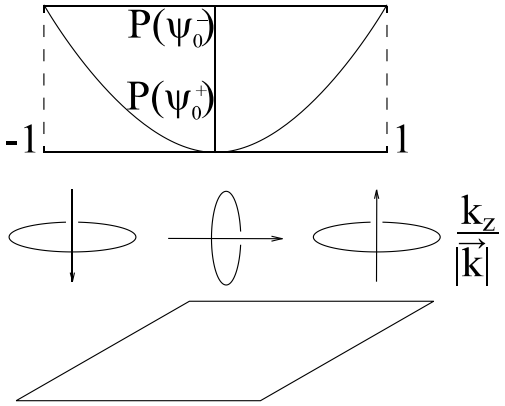


**Fig. 10.** Selection rules of the quantum transitions in both circular polarizations from the ground state of the crystal to the superposition magnetoexciton states $\left|\psi_0^{\pm}\left(\vec{k}_{\|}\right)\right\rangle$.

We will now discuss the case of light with linear polarizations $\vec{s}_{\vec{k}}$ and $\vec{t}_{\vec{k}}$ shown in Fig. 11.

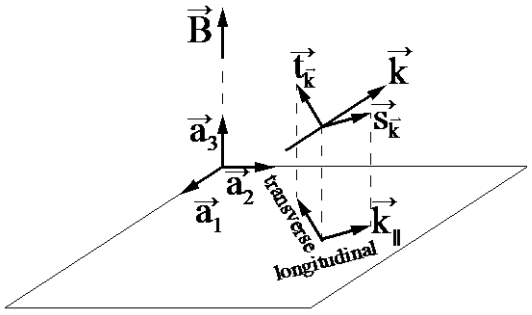


**Fig. 11.** Selection rules of the quantum transitions in two linear polarizations.

The probability of quantum transitions depends on the projections of the linear polarization vector $\vec{s}_{\vec{k}}$ and $\vec{t}_{\vec{k}}$ on the plane of the layer, especially on the fact whether they are longitudinal or transverse as regards the exciton in-plane wave vector $\vec{k}_{||}$. The symmetric superposition state is dipole active in the linear polarization $\vec{s}_{\vec{k}}$ with a longitudinal projection and forbidden in the linear light polarization $\vec{t}_{\vec{k}}$ with a transverse projection. As in the case of circular polarizations, the probability of quantum transitions is proportional to $k_z^2/|\vec{k}|^2$. The asymmetric superposition state is dipole active in the linear polarization $\vec{t}_{\vec{k}}$ with a transverse projection and forbidden in the $\vec{s}_{\vec{k}}$ polarization, and it does not depend on the light orientation. The probabilities of quantum transitions in the exciton states of the TMDC monolayers under the action of the linearly polarized light also depend on the projections of the polarization vectors on the surface of the monolayers, as in the case of the 2D magnetoexcitons. More so, this marvelous property has been first discussed and underlined by the authors of theoretical and experimental studies published in [1].

## 5. Conclusions

The influence of the e–h exchange Coulomb interaction on the superposition states formed by two 2D magnetoexciton with quantum numbers $F = \pm 1$, as well as by two valley Wannier–Mott excitons created in the TMDC monolayers, leads to the arising of new superposition exciton states with Dirac cone dispersion laws. A necessary condition for the implementation of this property is the interdependence between the center-of-mass and the relative e–h motions. In the case of magnetoexcitons, this interdependence is induced by the Lorentz force, whereas in the case of TMDCs, it is attributed to the existence and superposition of the exciton states in two equivalent valleys $\vec{K}$ and $-\vec{K}$ of the hexagonal Brillouin zone.

## References

[1] Y. Hongyi, L. Gui-Bin, G. Pu, X. Xiaodong and Y. Wang, Nat. Commun. 5, 3876 (2014).doi: 10.1038/ncomms4876
[2] S. Moskalenko, I. Podlesny, I. Zubac and B. Novikov, Solid State Commun. 302, 113714 (2019).
[3] S.A. Moskalenko and D.W. Snoke, Bose-Einstein Condensation of Excitons and Biexcitons and Coherent Nonlinear Optics with Excitons, Cambridge University Press, New York, 2000, p. 189.
[4] P.C. Hohenberg. Phys. Rev. 158, 383(1967). https://doi.org/10.1103/PhysRev.158.383
[5] H. Deng, H. Haug, and Y. Yamamoto, Rev. Mod. Phys. 82, 1489 (2010). https://doi.org/10.1103/RevModPhys.82.1489
[6] S.A. Moskalenko and I.M. Tiginyanu, Low Temperature Physics/Fizika Nizkikh Temperatur, 42, 5, 426-437 (2016). https://doi.org/10.1063/1.4948615
[7] S.A. Moskalenko et al., Phys. Rev. B 79, 125425 (2009).https://doi.org/10.1103/PhysRevB.79.125425
[8] S.A. Moskalenko et al., Solid State Commun. 283, 14(2018).https://doi.org/10.1016/j.ssc.2018.08.005.